Electronic Supplementary Material (ESI) for Soft Matter.


# Electronic Supplementary Information

# Unravelling topology-induced shape transformations in dendrimersomes

*Nina Yu. Kostina,[a‡] Anna M. Wagner,[a‡] Tamás Haraszti,[a] Khosrow Rahimi,[a] Qi Xiao,[b,c] Michael L. Klein,[c] Virgil Percec,[b] and Cesar Rodriguez-Emmenegger[*a]*

[a] DWI- Leibniz Institute for Interactive Materials, Forckenbeckstraße 50, 52074 Aachen, Germany

[b] Roy & Diana Vagelos Laboratories, Department of Chemistry, University of Pennsylvania, Philadelphia, PA 19104-6323, United States.

[c] Institute of Computational Molecular Science, Temple University, Philadelphia, PA 19122, United States.

E-mail: rodriguez@dwi.rwth-aachen.de

## Materials and Methods

### Materials.

Tetrahydrofuran (THF, dried over molecular sieve) and ethanol were purchased from Acros Organics while acetonitrile (MeCN) was purchased from Chemsolute. Difluoro[2-[1-(3,5-dimethyl-2H-pyrrol-2-ylidene-N)ethyl]-3,5-dimethyl-1H-pyrrolato-N]boron (BODIPY FL) was obtained from Sigma Aldrich. Silicon wafers (100 ± 0.3 mm diameter and 525 ± 20 µm thickness) were provided from Siegert Wafer and Secure-Seal™ Spacers (13 mm diameter and 0.12 mm thickness) were purchased from Thermo Fisher Scientific. Chromafil® provided Polytetrafluoroethylen (Teflon) syringe filter (0.2 µm pore size and 13 mm membrane diameter). High precision microscope cover glasses No. 1.5H (170 ± 5 µm thickness) were purchased from Marienfeld.

### Characterization methods of JDs.

**High Resolution Electrospray Ionization Mass Spectrometry (HRESI-MS**). The effect of irradiation on the structure of $JD^{pa}$ is investigated by analysis of the fragments of $JD^{pa}$ after irradiation in high-resolution ESI-TOF. Mass spectra were recorded using a micrOTOF-QII instrument from Bruker Daltonik (Billerica, Massachusetts). $JD^{pa}$ was dissolved in MeCN (5 $mg \cdot mL^{-1}$) and treated with UVB irradiation (280 – 315 nm) using an UV reactor for 16 h at room temperature. Prior to measurement the UVB treated sample was filtered using a polytetrafluoroethylene (Teflon) syringe filter (0.2 µm pore size and 13 mm membrane diameter). The identical solution of $JD^{pa}$ in MeCN was kept in dark conditions and used as a control sample.

**Geometry Optimization Simulation.** The quantum mechanical calculation was performed using the VAMP module in Accerlrys Material Studio 2017 (San Diego, California). An isolated molecule of $JD^{pa}$, $JD^{ps}$ and w-$JD^{pa}$ respectively was geometrically optimized by applying a permittivity of water of $\varepsilon$ = 78.54 $F \cdot m^{-1}$.

**Self-assembly of JDs into DSs.**

**Thin film rehydration method.** DSs were prepared by thin film rehydration the following way: $JD^{pa}$ (1218.53 $g \cdot mol^{-1}$) and $JD^{ps}$ (1882.50 $g \cdot mol^{-1}$) were dissolved in THF (100 µL, 10 $mg \cdot mL^{-1}$) and mixed at the molar ratios of 100/0, 70/30, 40/60, 10/90 and 1/99. Samples used in CLSM measurements were prepared by adding BODIPY-FL to the THF solution of JDs (0.5 mol%, 0.2 $mg \cdot mL^{-1}$, 262.11 $g \cdot mol^{-1}$). The JD solution was deposited on a roughened Teflon plate (1 cm x 1 cm) and the solvent was left to evaporate under ambient conditions for 2 h. The Teflon plates were transferred into a flat-bottom vial and dried *in vacuo* for additional 3 h. Milli-Q® water was added to the dried JD film for a final JD concentration of 1 $mg \cdot mL^{-1}$ and then hydrated in the oven at 60 °C over 12 h. Dispersions of the DSs DS-100, DS-70, DS-40, DS-10 and DS-1 were obtained after shaking by hand for 20 s. The measurements for the chosen compositions are depicted in Table 1.

**Table 1**. Calculation of five different compositions of DSs composed of $JD^{pa}$ and $JD^{ps}$ prepared by thin film rehydration method. Fluorescent BODIPY was added prior to CLSM experiments.

| | $JD^{pa}$ [mol%] | $V(JD^{pa})$ [µL] | $JD^{ps}$ [mol%] | $V(JD^{ps})$ [µL] | $V$(BODIPY-FL) [µL] | $V$(Milli-Q®) [µL] |
|---|---|---|---|---|---|---|
| DS-100 | 100 | 100 | 0 | 0 | 5.3 | 1000 |
| DS-70 | 70 | 60.2 | 30 | 39.0 | 4.5 | 992 |
| DS-40 | 40 | 30.4 | 60 | 69.0 | 4.0 | 994 |
| DS-10 | 10 | 6.8 | 90 | 93.0 | 3.6 | 998 |
| DS-1 | 1 | 0.7 | 99 | 99.0 | 3.5 | 997 |

**Injection method.** For cryo-TEM measurements, DSs were prepared by injection following the general method.[1] The respective solutions of $JD^{pa}$ and $JD^{ps}$ in THF (100 µL, 10 mg·mL$^{-1}$) were mixed in the molar ratios 100/0, 70/30, 40/60 and 10/90. The solution was injected into water (Milli-Q®) (0.5 mg·mL$^{-1}$) and vortexed for 20 s, respectively. Dispersions of the DSs I-DS-100, I-DS-70, I-DS-40 and I-DS-10 were obtained according to Table 2.

**Table 2**: Calculation of four different compositions of DSs composed of $JD^{pa}$ and $JD^{ps}$ prepared by injection method. Fluorescent BODIPY was added prior to CLSM experiments.

| | JDpa [mol%] | V(JDpa) [µL] | JDps [mol%] | V(JDps) [µL] | V(Milli-Q®) [µL] |
|---|---|---|---|---|---|
| I-DS-100 | 100 | 100 | 0 | 0 | 2000 |
| I-DS-70 | 70 | 60.2 | 30 | 39.0 | 1984 |
| I-DS-40 | 40 | 30.4 | 60 | 69.0 | 1989 |
| I-DS-10 | 10 | 6.8 | 90 | 93.0 | 1997 |

To investigate the mechanism of cleavage I-DS-100 was imaged in cryo-TEM before and after UV-Vis irradiation. The product of cleavage was analyzed after treating I-DS-100 dispersion in water with UVB irradiation in an UV reactor for 8 h (Figure S3).

**Characterization methods of DSs.**

**Optical Microscopy.** Optical microscopy was chosen to characterize vesicle shapes before and after UV irradiation. Images were recorded in Bright field (BF) and polarized (Pol) mode using a Zeiss Axioplan 2 imaging microscope (Oberkochen, Germany) with a 20x/0.50 objective and the corresponding 20x/0.50 Epi + DIC slider. Prior to measurement the DSs dispersion (20 µL, 1 mg·mL$^{-1}$) was deposited on a cleaned silicon substrate and sealed with Secure-Seal$^{TM}$ spacers (13 mm diameter, 0.12 mm thickness) between glass slides.

**Confocal Laser Scanning Microscopy (CLSM).** In CLSM a real-time study of the shape transformations of vesicles during UV irradiation was performed. Images and videos were recorded using a Leica TCS SP8 confocal microscope (Wetzlar, Germany) with a 100x/1.40 oil-immersion objective and a HyD detector. Since BODIPY-FL was used as a fluorophore, an excitation wavelength of 488 nm and an emission range of 507-570 nm were used to observe the vesicles. To visualize the shape transformation of DSs in real-time the samples were irradiated by a diode with $\lambda$ = 405 nm. All measurements were carried out at a constant temperature of 22 °C. The samples were prepared by deposition of DSs dispersion (20 µL, 1 mg·mL$^{-1}$) between two high precision microscope cover glasses (170 ± 5 µm) that were sealed with Secure-Seal$^{TM}$ spacers (13 mm diameter, 0.12 mm deep). All images were corrected in brightness and contrast and cropped using the Fiji-ImageJ software. Images showing smectic ordered vesicles and their shape transformation were further processed using the Tikhonov-Miller deconvolution algorithm with five iterations in the DeconvolutionLab2 Plugin for Fiji-ImageJ.[2]

**Cryogenic Transmission Electron Microscopy (cryo-TEM).** Cryo-TEM enables the study of vesicle morphologies before and after irradiation treatment. Images were recorded using a Zeiss LibraTM 120 transmission electron microscope (Oberkochen, Germany) in cryogenic mode. The measurement was carried out at a temperature of −170 °C and with an applied electron beam acceleration voltage of 120 kV. The samples were prepared using a FEI Vitrobot (Model Mark IV) plunge freezing station where the aqueous DSs dispersion (4 µL, 1 mg·mL$^{-1}$) was applied on plasma-treated lacey grids. After blotting and shock freezing in liquid ethane, the sample was fixed on a Model 910 cryo transfer specimen holder from Gatan (Pleasanton, California).

**Cryogenic Field Emission Scanning Electron Microscope (cryo-FESEM).** Images were recorded using a HITACHI S-4800 instrument (Tokio, Japan) in cryogenic mode with an applied electron beam acceleration voltage of 1 kV and a current of 2 µA. For the sample preparation, an ALTO2500 057 cryogenic preparation system was used. DSs dispersion (10 µL, 1 mg·mL$^{-1}$) was deposited on a rivet and shock frozen in liquid nitrogen. To image the inner morphology of the DSs, the sample was fractured in half using a blade included in the preparation chamber at a temperature of −145 °C. After transferring the sample into the observation chamber the sample was sublimated for one minute at a temperature of −80 °C prior to imaging in order to reduce residual ice on the surface.

**Wide Angle X-Ray Scattering (WAXS).** WAXS was employed to investigate the ordering and periodicity of supported bilayers. Spectra were recorded using an Empyrean setup from PANalytical (Almelo, Netherlands). Cu$K_\alpha$ radiation (40 kV, 40 mA) with a characteristic wavelength of $\lambda$ = 0.1542 nm was chosen. The scattered signal was recorded as a function of the scattering angle 2θ. The scattering angle was converted to the scattering vector q, using $q = 2\pi/d = (4\pi/\lambda) \sin(\theta)$. The spectra were further background corrected by comparing to a <111> Si surface. The resolution limit was determined by measuring a high-quality silicon wafer that resulted in a resolution-limited peak with a full-width-at-half-maximum of 25 mdeg. The sample was prepared by depositing DSs dispersion (50 µL, 1 mg·mL$^{-1}$) on a cleaned and hydrophilized <111> silicon substrate.

# Supplementary results

**HRESI-MS.**

Irradiation with UV-Vis light ($\lambda$ = 405 nm) cleaves the *o*-nitrobenzyl (NB) group of JD$^{pa}$. The cleavage results in two fragments, a hydrophilic dendron Dn$^{hydrophil}$ containing an acid moiety and a weakly amphiphilic minidendron w-JD$^{pa}$ with an aldehyde moiety (*o*-nitrosobezaldehyde-derivative).

High resolution electrospray ionization mass spectrometry (HRESI-MS) was conducted for a JD$^{pa}$ in MeCN solution before and after irradiation. A background of the solute system was recorded and subtracted from each measurement. The high-resolution mass spectrum with a subtracted background obtained from the solution of JD$^{pa}$ in acetonitrile before irradiation is depicted in Figure S1 A. The highest intensity peak at *m*/*z* = 1268.7286 corresponds to non-cleaved JD$^{pa}$ with a calculated mass-to-charge-ratio of $[M+Na]^+ = [C_{67}H_{107}NO_{20}Na]^+ = 1268.7284$.

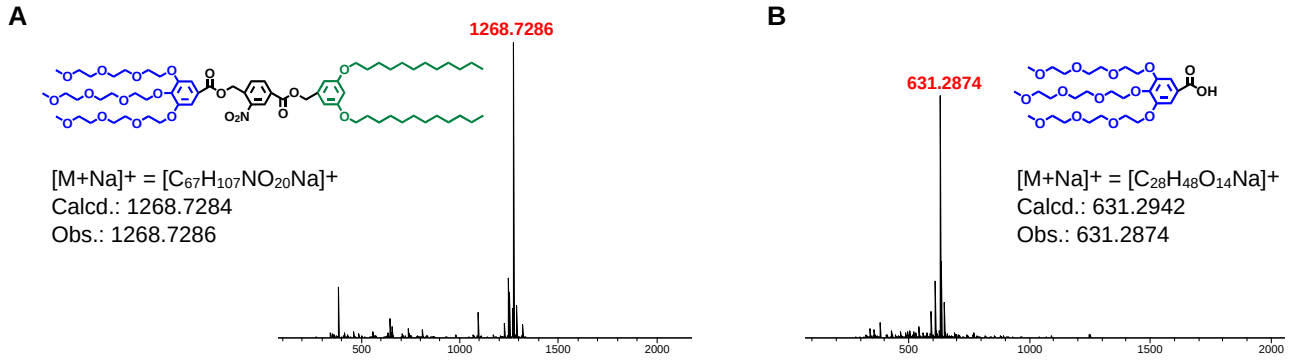


**Figure S1**. (A) Background subtracted high-resolution mass spectrum before cleavage of the JD$^{pa}$ in acetonitrile solution (5 mg·mL$^{-1}$) and (B) after cleavage (280 - 315 nm, 16 h, rt) and separation of precipitant.

During the irradiation of a JD$^{pa}$ acetonitrile (MeCN) solution (5 mg·mL$^{-1}$) with UVB light (280 - 315 nm, 16 h, rt) the fragment w-JD$^{pa}$ precipitated due to its hydrophobic nature. The fragment w-JD$^{pa}$ was filtered off through a PTFE syringe filter (0.2 µm pore size) leaving only the soluble fractions for analysis. The corresponding high-resolution mass spectrum after irradiation with a subtracted background is depicted in Figure S1 B. The highest intensity peak at *m*/*z* = 631.2874 corresponds to the hydrophilic dendron Dn$^{hydrophil}$ with the theoretical m/z of $[M+Na]^+ = [C_{28}H_{48}O_{14}Na]^+ = 631.2942$. A full cleavage of all JD$^{pa}$ molecules was confirmed since no peak corresponding to the non-cleaved JD$^{pa}$ was found. Moreover, the precipitant containing w-JD$^{pa}$ was successfully separated since no peak at the exact mass of $m[C_{39}H_{59}NO_7] = 653.4292$ was detected.

**WAXS.**

The presence of a lamellar mesophase was confirmed by wide-angle X-ray scattering (WAXS). Prior to measurement a DS-10 water dispersion was left to dry on a silicon substrate at ambient conditions. During the drying process the DSs are expected to form a stack of bilayers on the silicon substrate with a periodicity according to the bilayer thickness. The scattering curve is presented in Figure S4 after a background correction by subtracting the scattering of a blank silicon substrate.

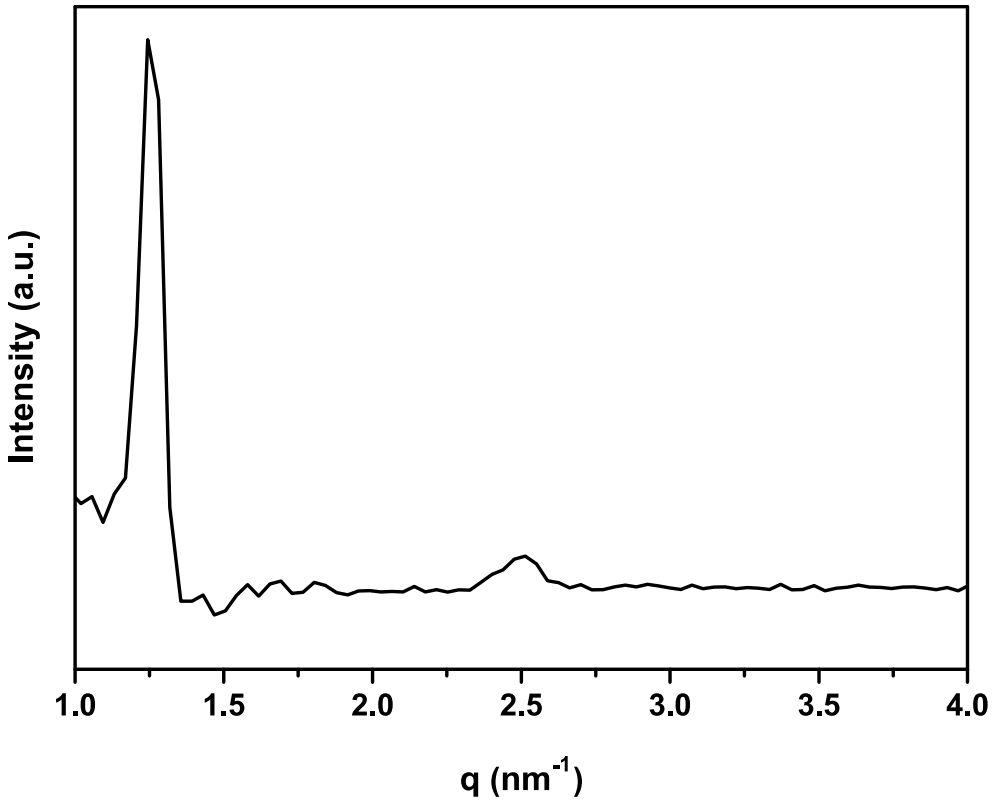


**Figure S2**. WAXS measurement of DSs with 10 % pa-JD with subtracted background.

Two scattering peak positions were observed at the scattering vectors $q$ = 1.24 nm$^{-1}$ and $q$ = 2.51 nm$^{-1}$, respectively with q/q* : 1:2 indicating a lamellar ordering. The corresponding lamellar thickness is about 5.05 nm.

## Characterization of DSs by cryo-TEM.

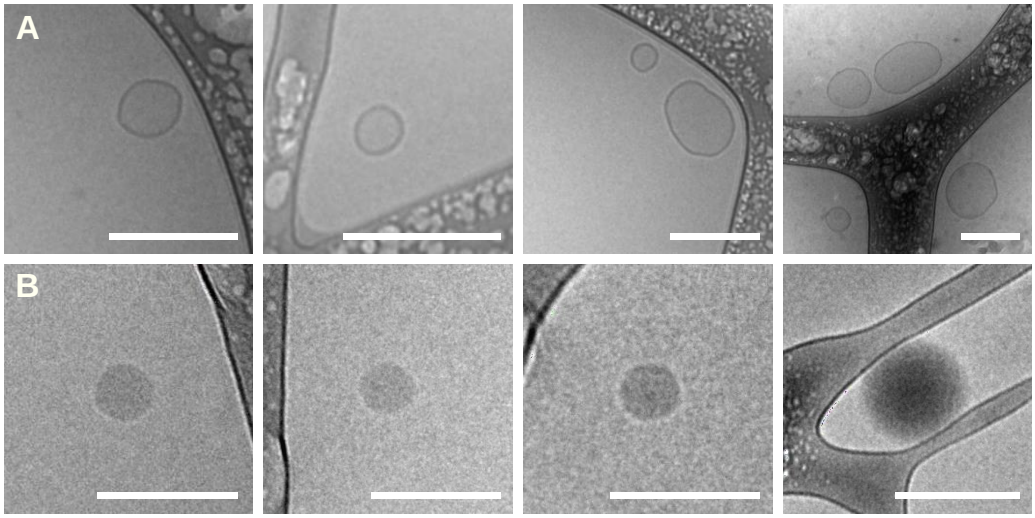


**Figure S3**. (A) Unilamellar vesicles after preparation of sample I-DS-100 according to the injection method observed in cryo-TEM without UVB treatment. (B) Aggregate formation after preparation of sample I-DS-100 according to the injection method observed in cryo-TEM irradiated with UVB (280 - 315 nm, 8h, rt.) after injection into water. The scale bar is 200 nm (A) and 100 nm (B).

## Characterization of DSs by optical microscopy.

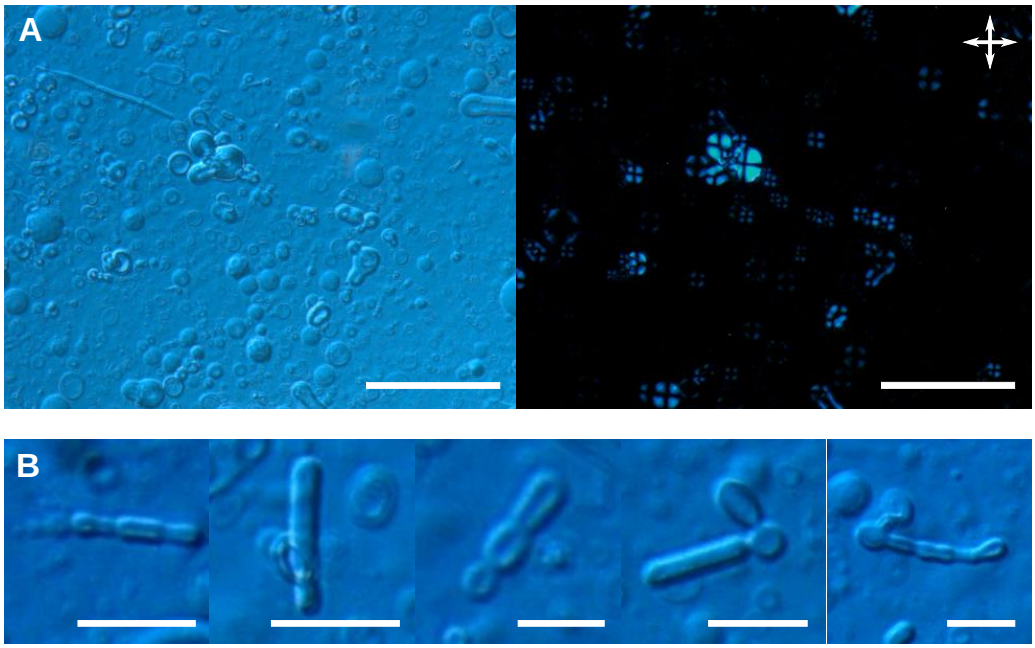


**Figure S4**. (A) Tube and necklace formation of DS-10 observed in optical microscopy after irradiation with UV-Vis with BF and Pol optical microscopy overview images and (B) enlarged images showing tubes and necklaces. The scale bar is 100 µm (A) and 20 µm (B).

## Characterization of DSs by CLSM

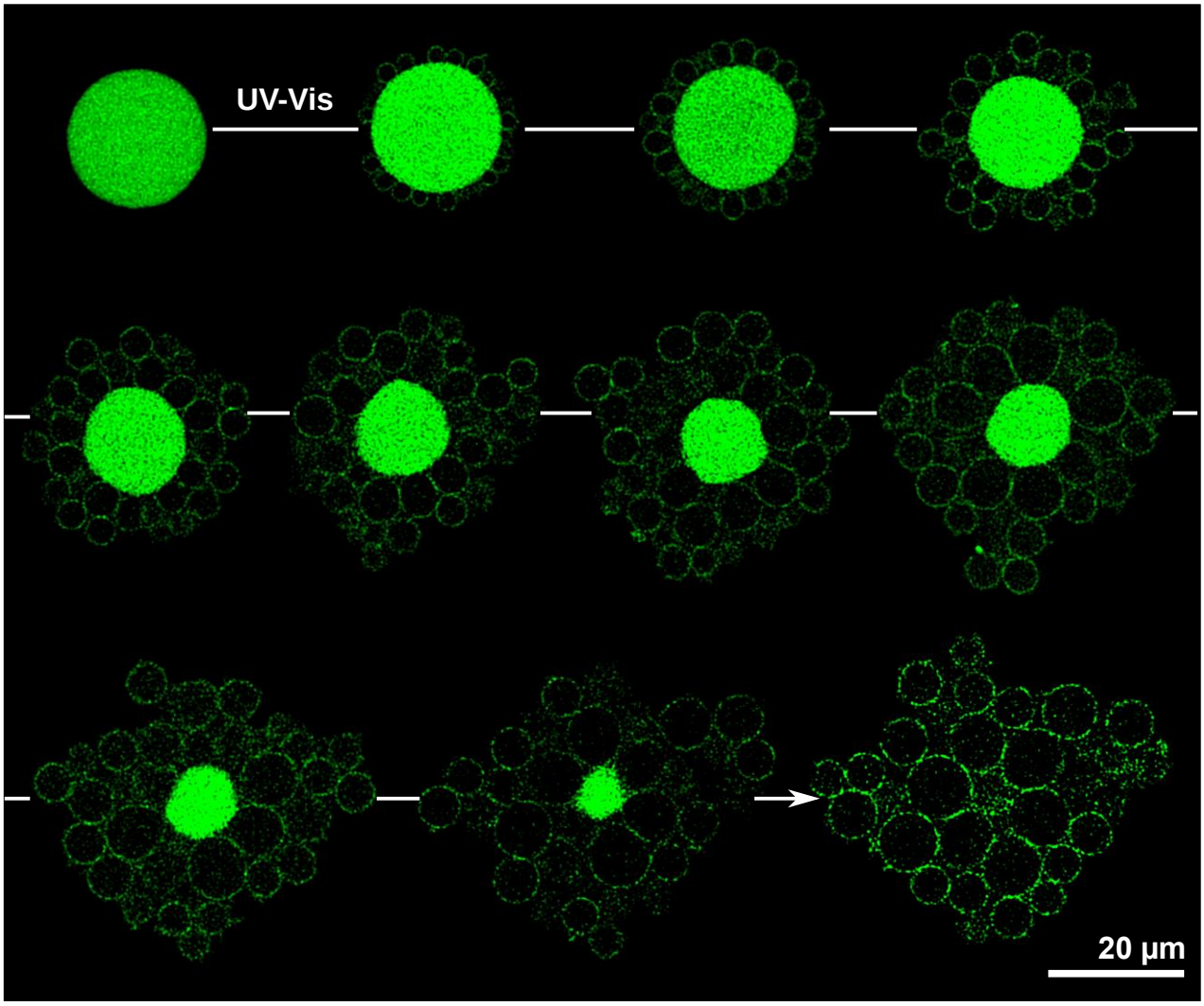


**Figure S5**. CLSM image sequence showing the formation of small daughter vesicles from a smectic-ordered DS-100 upon UV-VIS irradiation. Background in CLSM cropped.

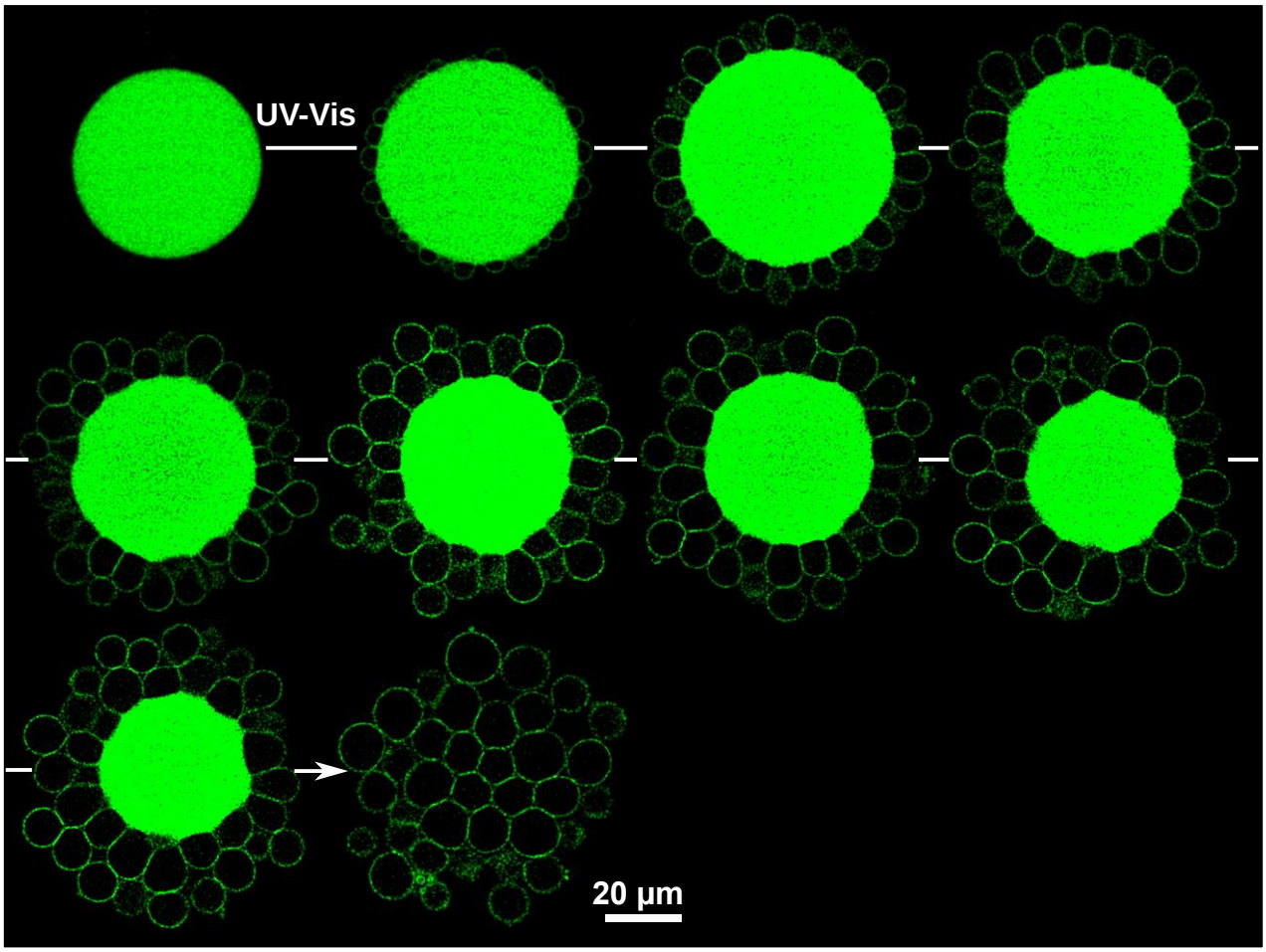


**Figure S6**. CLSM image sequence showing the formation of small daughter vesicles from a smectic-ordered DS-70 upon UV-VIS irradiation. Background in CLSM cropped.

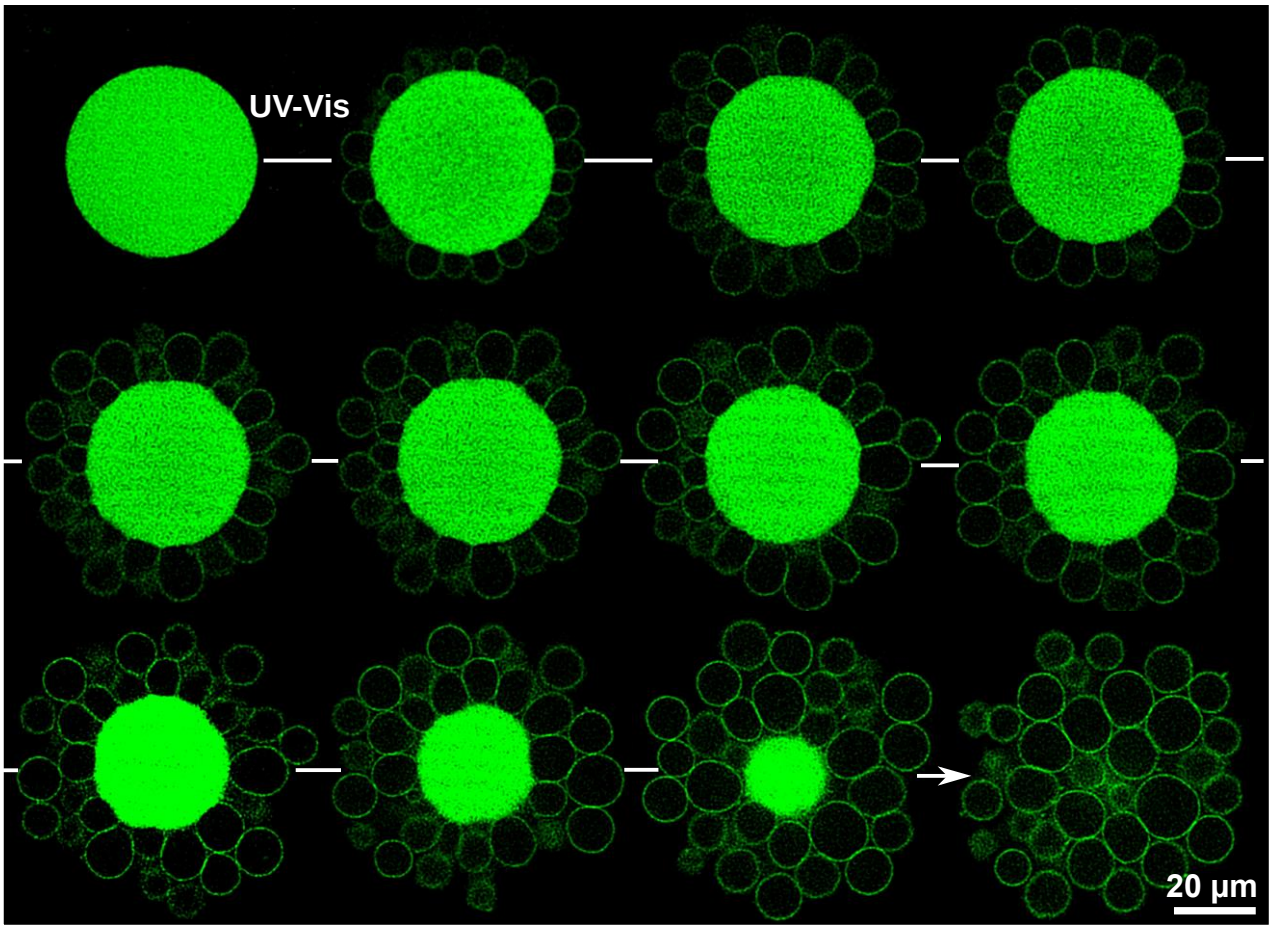


**Figure S7**. CLSM image sequence showing the formation of small daughter vesicles from a smectic-ordered DS-40 upon UV-VIS irradiation. Background in CLSM cropped.

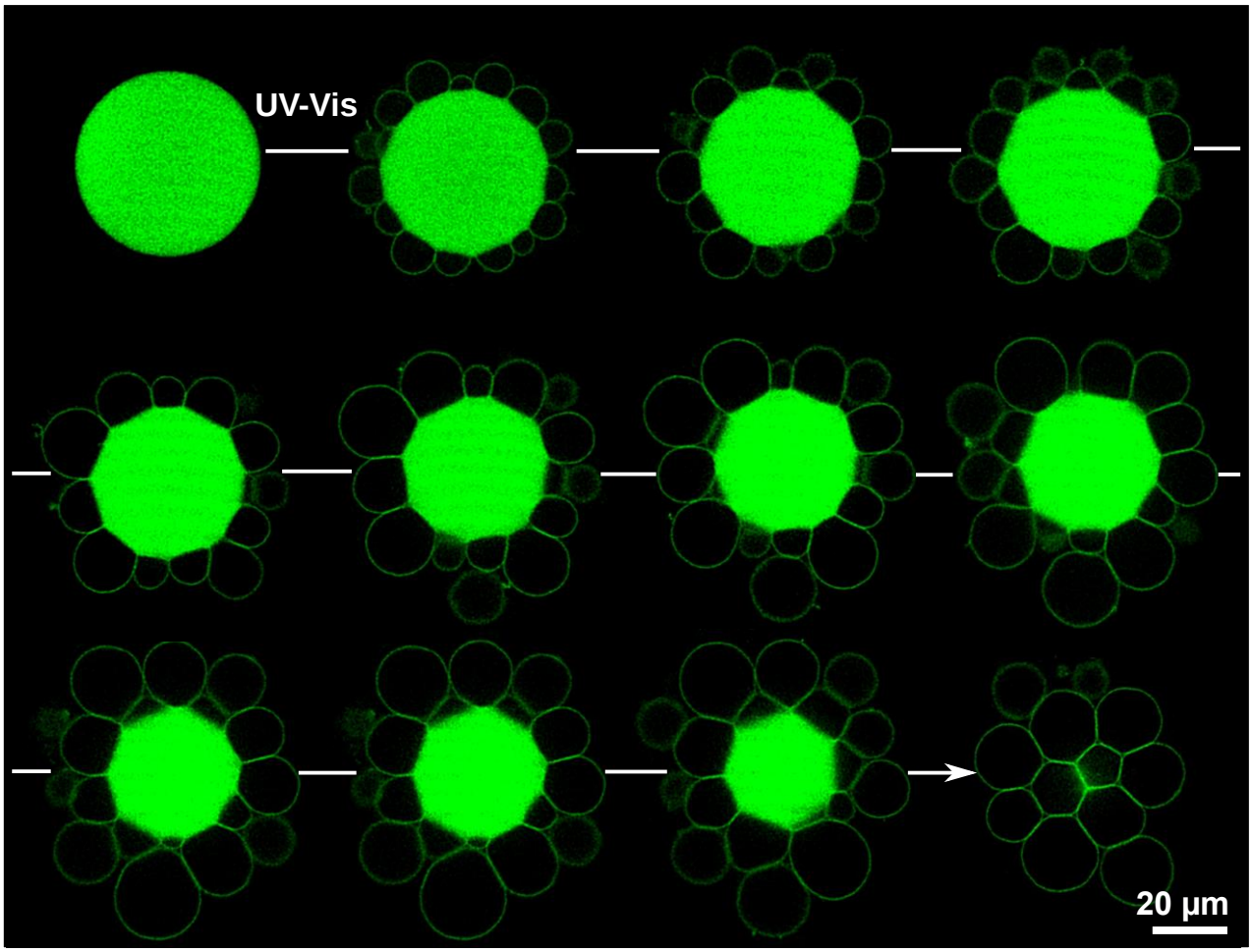


**Figure S8**. CLSM image sequence showing the formation of small daughter vesicles from a smectic-ordered DS-10 upon UV-VIS irradiation. Background in CLSM cropped.

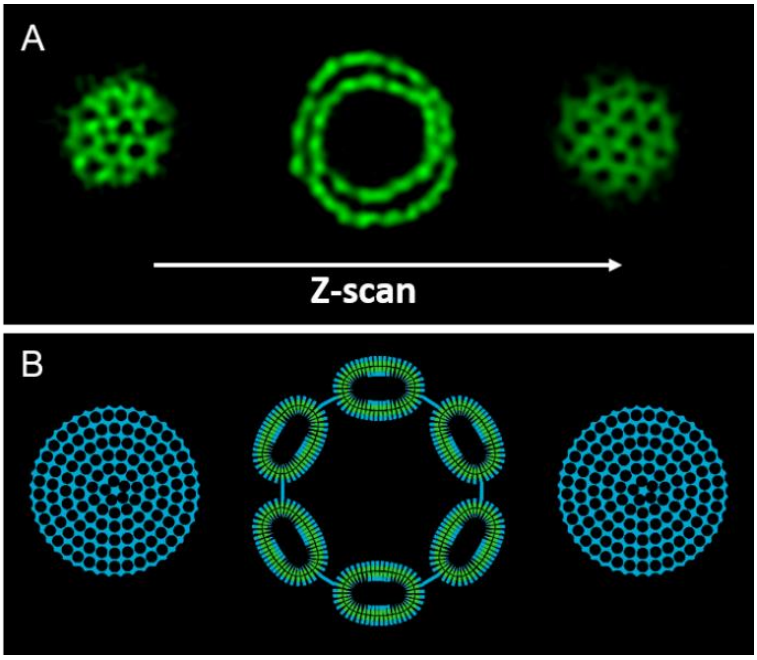


**Figure S9**. (A) A Z-scan in CLSM displays the top, the cross-sectional area and the bottom plane of a multilamellar DS-10 after irradiation with UV-Vis and (B) a schematic representation of the pore formation. Background in CLSM cropped.

**Analysis of membrane fluctuations**

Image processing of CLSM image stacks was performed in python following a general procedure. The stack was cropped to the region of interest and split up to individual images. Background images were generated for each image by blurring the images via convolution of a Gaussian kernel (window typically 61 pixels, width $\sigma$ = 10 pixels). The background was subtracted from the original image, and resultant negative pixels were set to zero. The image was then smoothed with a second Gaussian kernel (window size = 11 pixels and width $\sigma$ = 1 pixels). A binary image was generated from the result by applying a threshold which was calculated according to Otsu's method.[3] The binary image was then scanned and confluent objects with a predefined size range were selected. This size range was adjusted to the specific image stack, ranging typically from 500-1100 pixels area minimum and 2000-5000 pixels area maximum. The resulting objects were then filled back with a corrected background and smoothed intensity values. The center of mass defined the central of the object, and the pixel coordinates relative to this center were converted to polar coordinates, distance (or radius) and angle. Due to a relatively high number of pixels, an angle range was defined between 0 and $2\pi$ radians with as many numbers of points as the circumference of the average radius circle ($2\pi\langle r\rangle$). In each of the so defined angular bins the intensity weighted mean and standard deviation (first and second statistical momentum) of the distances (radii) were calculated.

To compare the angular profiles, first the mean radius was subtracted from each data set, resulting in Δr = r - <r>. In order to better visualize the fluctuations we removed the shape contributions.[4, 5] For this we first shifted the Δr(φ) so that the zero angle of all analyzed vesicles was at the maximum of the curve (main axis of a prolate). Then Δr(φ) was fitted with a sum of cosine functions with integer harmonics where $\varphi$ is the angle variable from the data:

$$\Delta r = \sum_{i=1}^{N} a_i \cdot cos(i\varphi)$$

The shape is generated by the two first harmonics of the cosine series, thus they were subtracted to Δr(φ) to generate Δr(φ)'.

The analysis was performed for DS-10 before and after irradiation and DS-70 after irradiation. Fig. S10 displays the selected vesicles and their fitting. The profiles are plotted in Fig. S11. DS-10 after irradiation show much higher fluctuations than before as evidenced in Fig. S11 C in line with the generation of w-$JD^{pa}$ upon irradiation. As expected increasing the ratio of $JD^{pa}$ in DS-70 resulted in even higher fluctuations. This highlights the effect of the molecular shape in the dynamics of the shape transition.

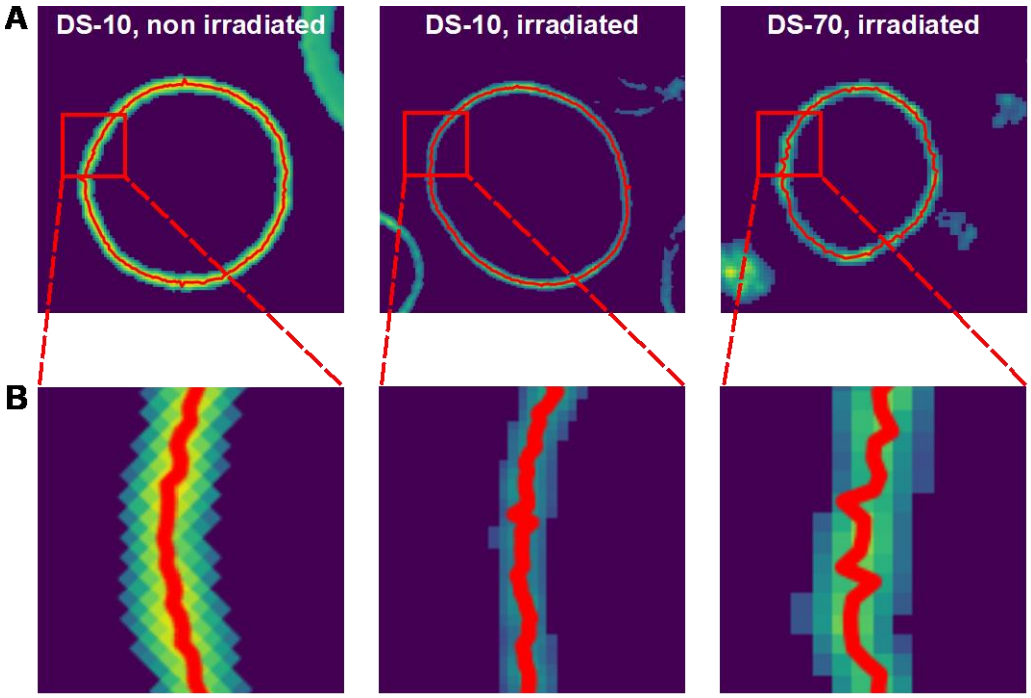


**Figure S10**. (A) CLSM images depict a unilamellar DS-10 vesicle before irradiation and DS-10 and DS-70 upon irradiation. (B) Magnification of the DS membrane shows increased membrane fluctuations with irradiation and with increasing ratio of $JD^{pa}$.

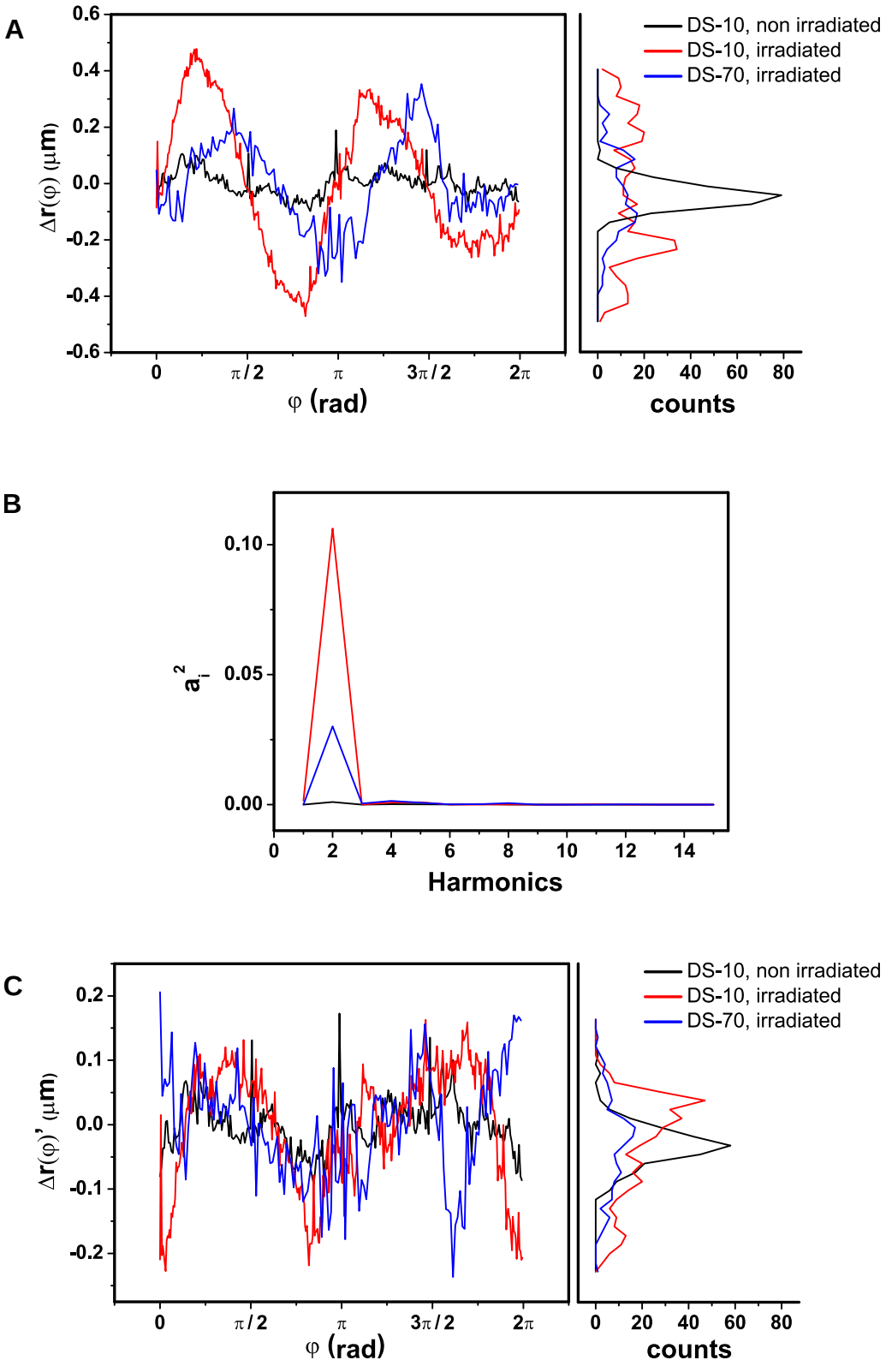


**Figure S11**. (A) Difference in angular fluctuation behavior and distribution of unilamellar vesicles upon irradiation or increase in ratio of $JD^{pa}$. (C) Angular fluctuation and distribution after subtracting the second harmonics of the cosine decomposition (B) shows the shape-independent higher order fluctuations after subtracting a second order series of cosines.

**Analysis of pore arrays in multilamellar vesicles.**

Upon irradiation multilamellar vesicles transition into high genus morphologies with membrane-linking pores (MLPs) in the order of g ~ 100. For a pore size and pore separation analysis CLSM images of each composition from DS-1 to DS-70 were processed following a general procedure. The background was corrected by using a Gauss deblur (window size and width were varied to detect as many of the holes as possible, with sizes of 61, 41 and 31 pixels, and widths σ = 10, 6 and 5 pixels respectively). The result was subtracted from the original image and negative values were rejected. Further, the images were smoothed by applying a second Gaussian (window sizes 17, 17 and 11 pixels, and widths σ = 2, 2 and 1 pixels respectively). A threshold was defined where all spots with less than 50 pixels or more than 1000 pixels were rejected. The inverted image was calculated where the values below the 0.4 quantile of the intensity distribution defined the pores in the hexagonal lattice. The number of pixels in each patch were used to calculate the pore radii by $A = \pi \cdot r^2$. The geometric center of the hole was calculated and used to analyze the distances between two pores and the order. For the former, the pore distances were limited within a circle of two times the closest neighbor where each pore had a maximum of six neighbors. For the latter, the local bond order parameter $\psi^6$ was calculated according to $\psi^6(\vec{r_i}) = \frac{1}{N_j}\sum_{j=1}^{N_j} e^{i6\theta_{ij}}$ with $N_j$ as the nearest neighbor number and θ as the angle from the neighbors to each other through the center to classify hexagonal patterns.[6]

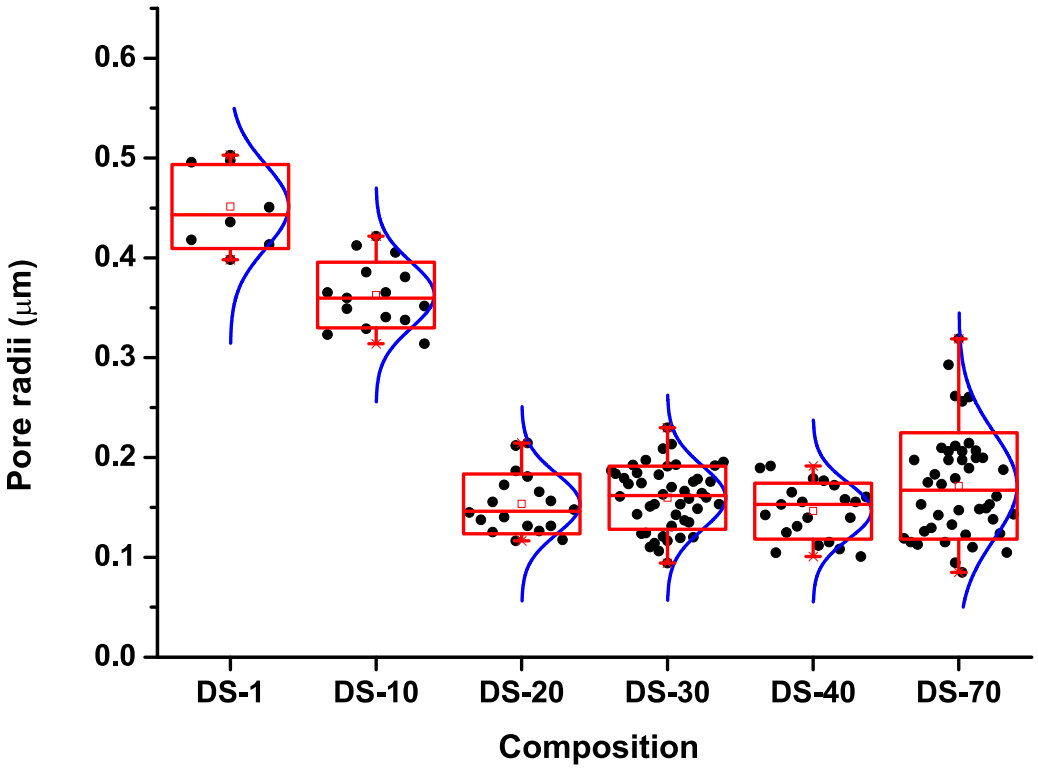


**Figure S12**. Boxplot of pore radii for different compositions. The blue curves represent the normal distribution to which the data is fitted. The box plot shows decreasing pore radii with increasing ratio of $JD^{pa}$ in high genus vesicles obtained upon irradiation of multilamellar vesicle types while compositions ranging from DS-20 to DS-70 reached a constant pore radius. Box region depicts the standard deviation and whiskers display minimal and maximal pore radius.

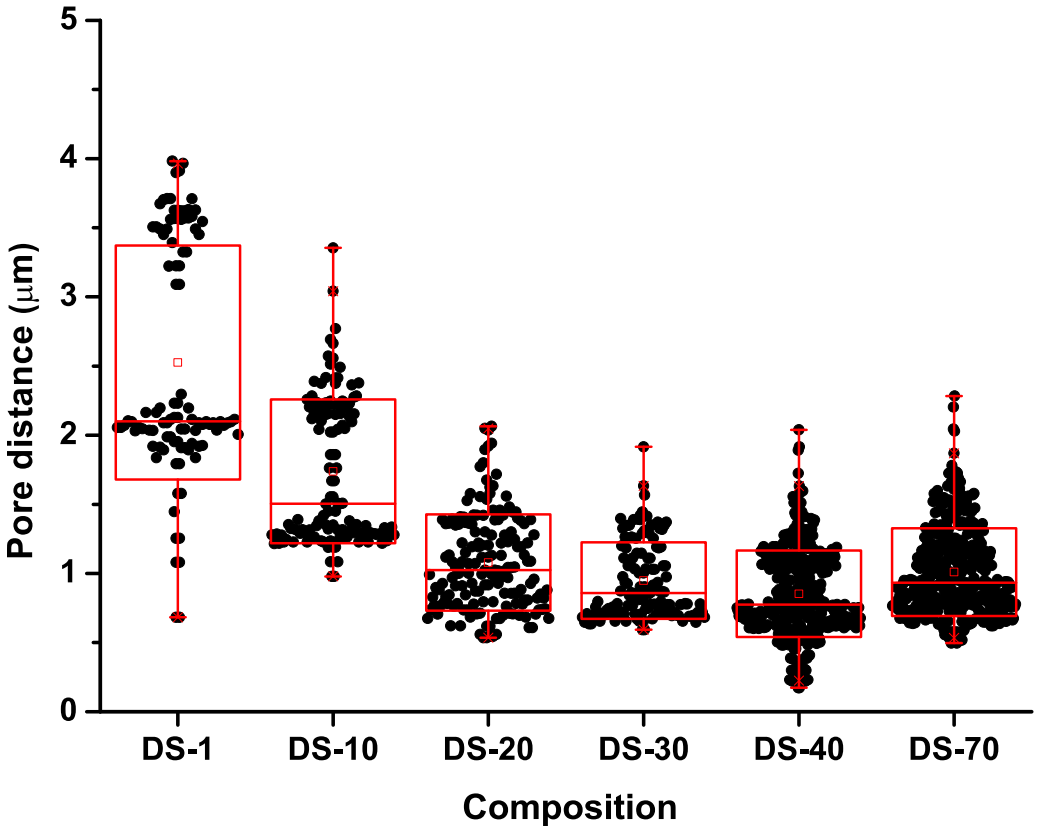


**Figure S13**. Boxplot of pore distances for different compositions. The box plot shows a decreasing pore separation (center-to-center distance) with increasing ratio of $JD^{pa}$ in high genus vesicles obtained upon irradiation of multilamellar vesicles. Box region depicts the standard deviation and whiskers display minimal and maximal pore radius.

**Analysis of daughter DS size from smectic-ordered vesicles.**

During the shape transformation of smectic ordered vesicles, budding resulted in the formation of smaller sized daughter vesicles around the whole surface of the smectic vesicle. CLSM images were recorded by locating the confocal plane in the equatorial plane of the DSs. For the analysis of the bud diameter a general calculation method was followed. The background of the original CLSM images was corrected by calculating the convolution with a broad Gaussian kernel (window size 61 pixels, width $\sigma = 10$ pixels). The obtained result was subtracted from the original CLSM images. A second Gaussian kernel (window size 21 pixels, width $\sigma = 3$ pixels) was used to reduce the high pixel-to-noise ratio and smoothen the images. An intensity threshold was applied to identify the structure area. For this purpose, all spots with less than 500 pixels or more than 150000 pixels were rejected. The rest was merged using a sequence (5 consecutive application) of binary dilation and then eroded back in a similar cycle. Patches

separated by membrane were identified in the inverse image. Images were dilatated to obtain the membrane segments. The obtained segments were fitted to a circle using an algorithm according to Taubin and Al-Sharadqah.[7, 8]

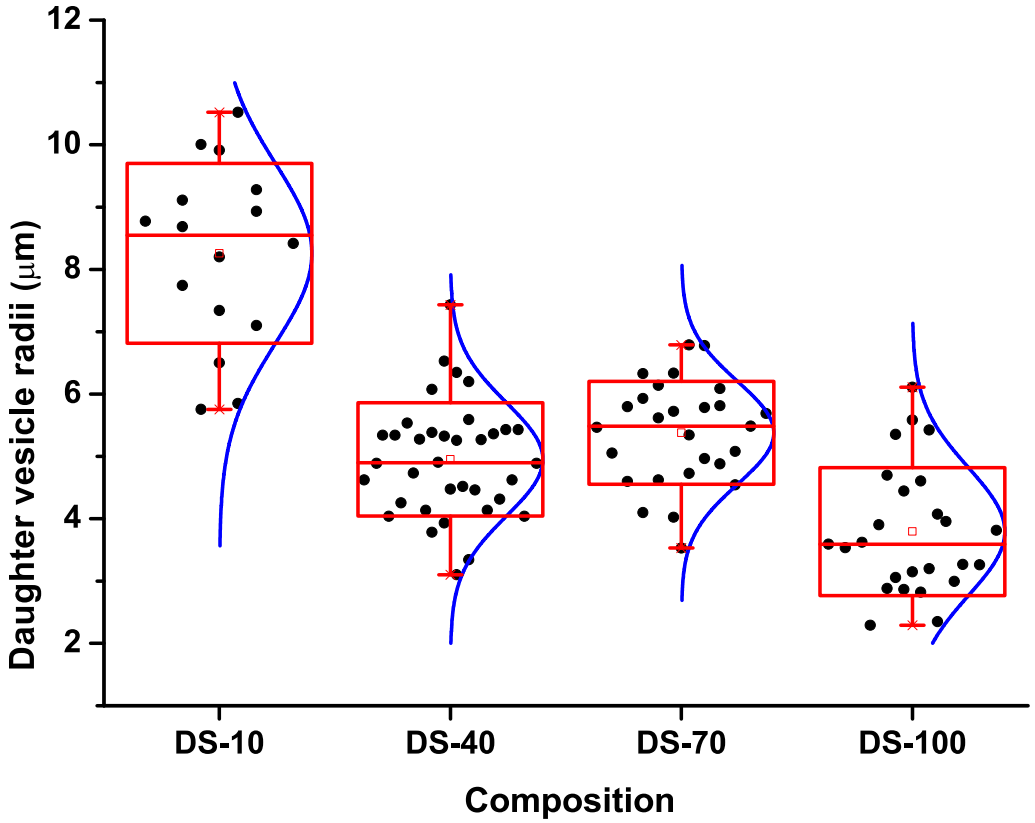


**Figure S14**. Boxplot of daughter vesicle radii for different compositions. The blue curves represent the normal distribution to which the data is fitted. The box plot shows decreasing daughter vesicle radii with increasing ratio of $JD^{pa}$ upon irradiation of smectic type vesicles. Box region depicts the standard deviation and whiskers display minimal and maximal pore radius.

**Analysis of the dimensionless effective spontaneous curvature $\bar{m}_{eff}$.**

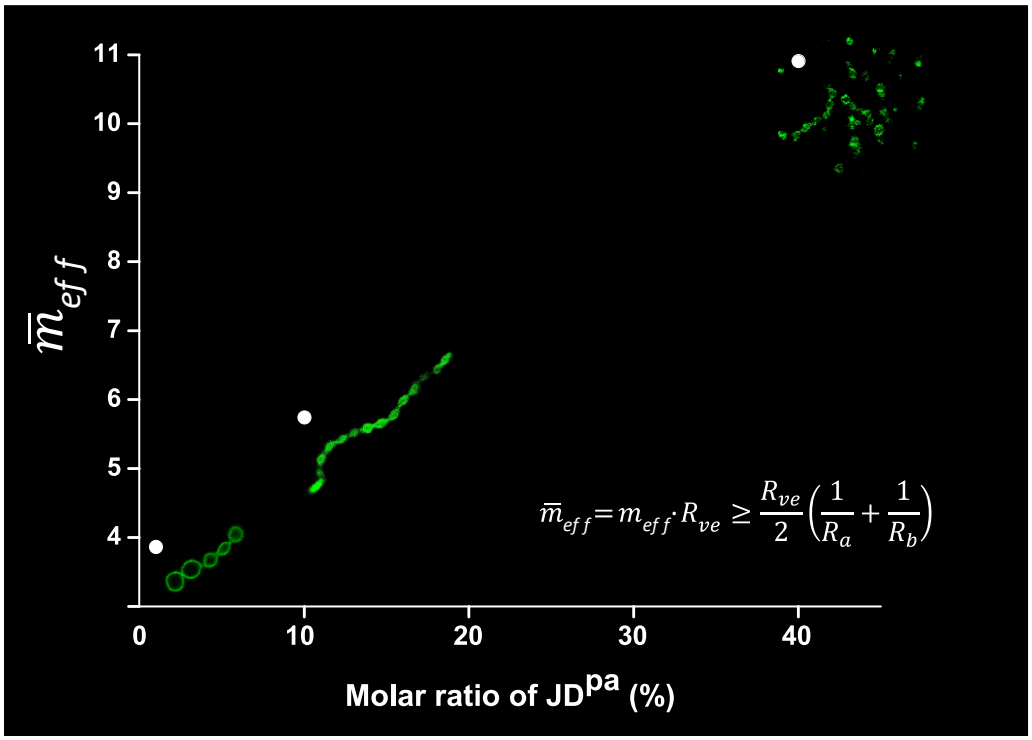


**Figure S15**. In unilamellar DSs the minimum value of the dimensionless effective spontaneous curvature $\bar{m}_{eff}$ was calculated based on the neck stability condition (equation shown) for three different compositions ranging from DS-10 to DS-40.

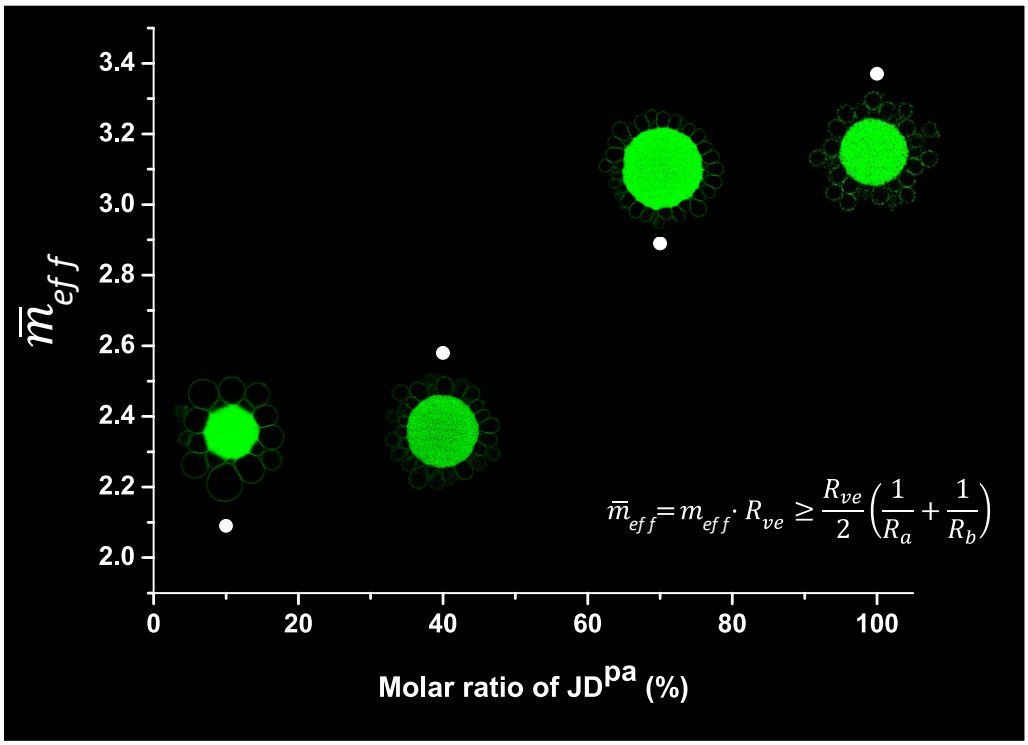


**Figure S16**. In smectic-ordered DSs the minimum value of the dimensionless effective spontaneous curvature $\bar{m}_{eff}$ was calculated based on the neck stability condition (equation shown) for four different compositions ranging from DS-10 to DS-100.

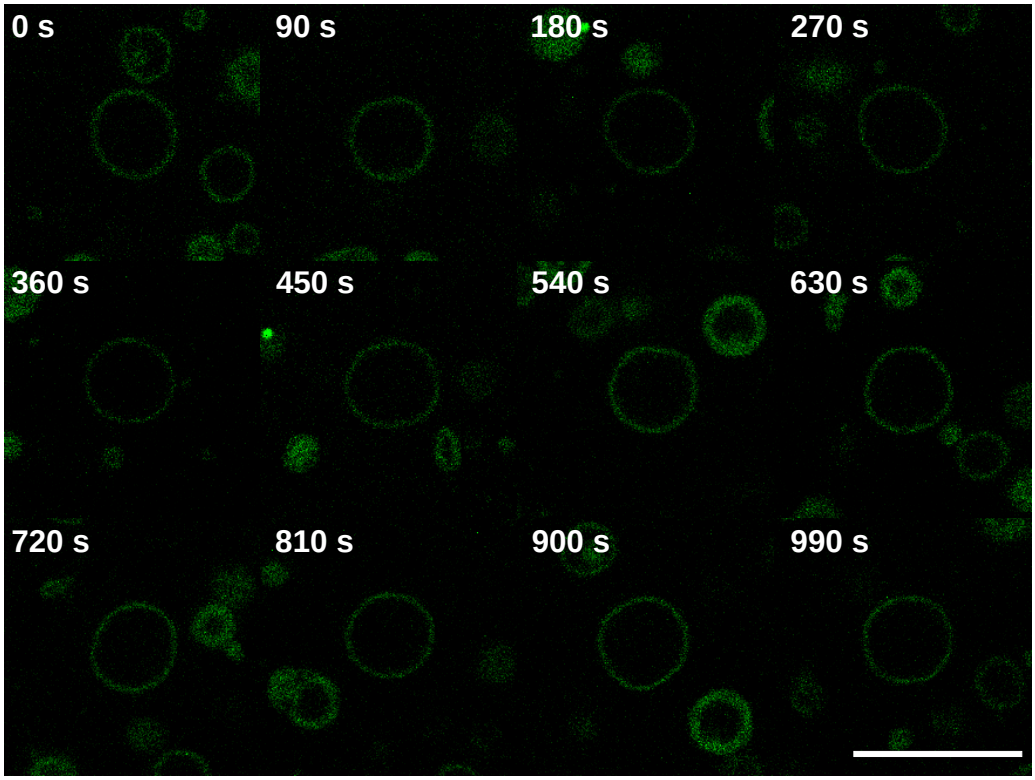


**Figure S17**. CLSM shows an unilamellar vesicle co-assembled from 100% $JD^{pa}$ (DS-100). The vesicle was followed without UV-Vis irradiation indicating no changes in shape over a time range of 990 s. The scale bar is 10 µm.

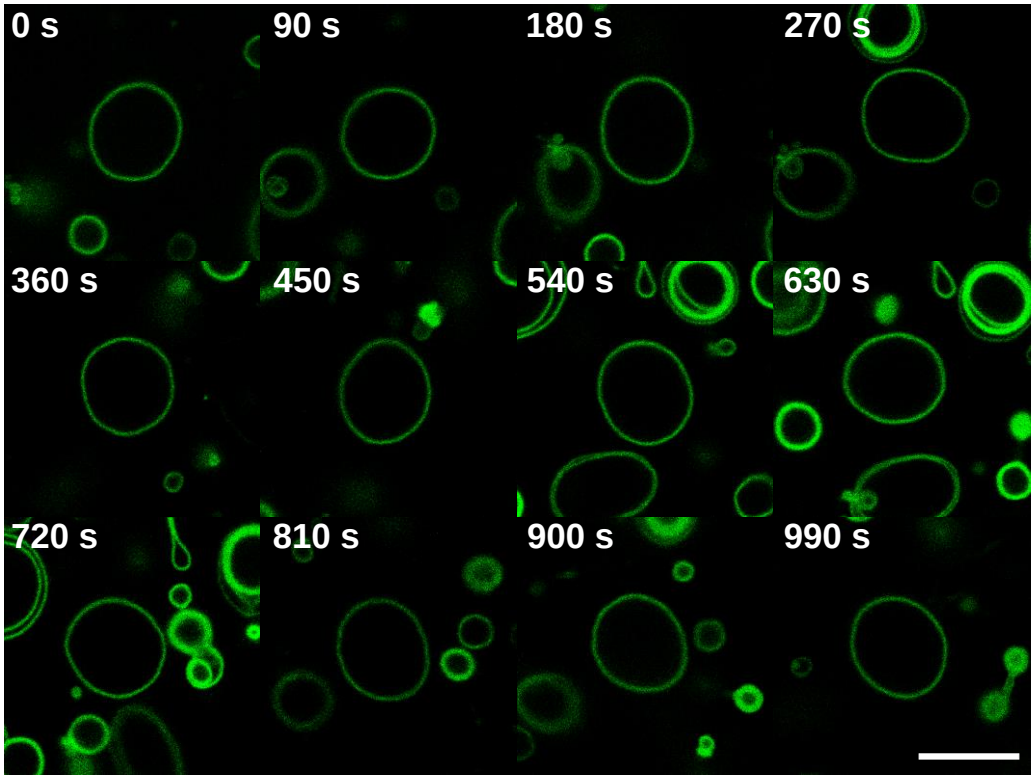


**Figure S18**. CLSM shows an unilamellar vesicle co-assembled from 100% $JD^{ps}$ (DS-0). The vesicle was followed with UV-Vis irradiation indicating no changes in shape over a time range of 990 s. The scale bar is 10 µm.

**References**


1. M. Pons, M. Foradada and J. Estelrich, *International Journal of Pharmaceutics*, 1993, **95**, 51-56.
2. D. Sage, L. Donati, F. Soulez, D. Fortun, G. Schmit, A. Seitz, R. Guiet, C. Vonesch and M. Unser, *Methods*, 2017, **115**, 28-41.
3. N. Otsu, *IEEE Transactions on Systems, Man, and Cybernetics*, 1979, **9**, 62-66.
4. H. P. Duwe and E. Sackmann, *Physica A: Statistical Mechanics and its Applications*, 1990, **163**, 410-428.
5. R. Dimova, *Adv. Colloid Interface Sci.*, 2014, **208**, 225-234.
6. A. E. Larsen and D. G. Grier, *Phys. Rev. Lett.*, 1996, **76**, 3862-3865.
7. G. Taubin, *IEEE Transactions on Pattern Analysis and Machine Intelligence*, 1991, **13**, 1115-1138.
8. A. Al-Sharadqah and N. Chernov, *Electronic Journal of Statistics*, 2009, **3**, 886-911.